Heliyon 10 (2024) e31909

Contents lists available at ScienceDirect

Heliyon

journal homepage: www.cell.com/heliyon

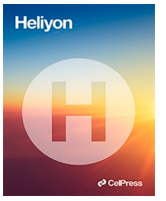

Research article

Shikonin-loaded PLGA nanoparticles: A promising strategy for psoriasis treatment

Jing Fu [a], Longtai You [b], Daohan Sun [a], Lu Zhang [a], Jingxia Zhao [a,**], Ping Li [a,*]

[a] Beijing Hospital of Traditional Chinese Medicine, Capital Medical University, Beijing Institute of Traditional Chinese Medicine, Beijing, 100010, China

[b] Department of Pharmacy, Beijing Children's Hospital, Capital Medical University, National Center for Children's Health, Beijing, 100045, China

ARTICLE INFO

Keywords:
Psoriasis
Shikonin
PLGA nanoparticles
Hydrogel
Proinflammatory cytokines

ABSTRACT

Psoriasis is an inflammation-based skin illness marked by aggravated proliferation of epidermal cells. Shikonin is a natural naphthoquinone obtained from *Arnebiae* radix. It exerts anti-inflammatory and immunosuppressive effects. However, the poor water solubility and low bioavailability of shikonin limit its application. In this study, shikosin-loaded PLGA nanoparticle hydrogel was prepared and used to deliver the drug to the epidermis of psoriasis mice through local administration. The results demonstrated that shikosin-loaded PLGA nanoparticles inhibited HaCaT cell multiplication, increased drug uptake, and induced apoptosis of HaCaT cells. Results from Western blotting assays indicated that shikosin down-regulated the protein expressions of p65 and p-p65. Furthermore, shikonin mitigated psoriasis and decreased the concentrations of inflammation-inducing cytokines, i.e., IL17A, IL-17F, IL-22, IL-1β, and TNF-α. Taken together, these results suggest that shikonin-PLGA nanoparticles loaded in hydrogel system possess promising therapeutic potential for psoriasis.

1. Introduction

Psoriasis is a disease caused by chronically-occurring inflammation of the skin [1,2]. The histopathological manifestations of psoriasis are mainly hyperkeratosis of keratinocytes in the basal layer of the epidermis, dilatation of dermal capillaries, and infiltration of inflammatory cells [3,4]. The psoriasis-related inflammation process is under the mediation of dendritic cells and T cells. These cells interact with epidermal keratinocytes, resulting in epidermal proliferation, hyper-keratinization and hypokeratosis; lymphocyte infiltration, and extensive angiogenesis [5,6]. Dendritic cells and T cells are immune cells that infiltrate the skin and produce large number of cytokines which stimulate keratinocytes. These cytokines are IL-17, IL-23, and IFN-γ. On activation, keratinocytes produce multiple pro-inflammatory cytokines, chemokines and anti-microbial peptides, thereby creating a vicious cycle that maintains and aggravates psoriasis [7,8]. Topical administration is the preferred approach for the therapy of psoriasis. Percutaneous drug absorption, an important method of drug administration in clinics, is used to prevent first-pass effect and gastrointestinal irritation, thereby ensuring that the drug directly reaches the disease site [9,10]. Although most topical drugs for psoriasis produce therapeutic effects, these effects are limited, resulting in disease recurrence. Moreover, long-term use of these drugs may result in poor patient compliance. Due to factors such as the barrier effect of the skin and the molecular weight of drugs, the transdermal absorption of drugs is low.

* Corresponding author.
** Corresponding author.
E-mail addresses: zhaojingxia@bjzhongyi.com (J. Zhao), liping@bjzhongyi.com (P. Li).

https://doi.org/10.1016/j.heliyon.2024.e31909
Received 15 March 2024; Received in revised form 22 May 2024; Accepted 23 May 2024
Available online 23 May 2024

Arnebiae radix has been used in China for more than two thousand years for *clearing heat* and *cooling the blood*, *activating blood*, detoxification, and elimination of rashes and spots [11–14]. It is a typical representative drug used for *cooling* and *activation of blood,* and for detoxification of psoriasis; it is vital for psoriasis therapy. Shikonin, a natural naphthoquinone compound, is one of the main bioactive compounds in *Arnebiae* radix [15–17]. In our previous study, it was shown that shikonin inhibited the multiplication of IL-17A-treated HaCaT cells and the secretion of related cytokines, thereby producing therapeutic effect on psoriasis. Moreover, it was demonstrated that shikonin inhibited the maturation of dendritic cells and the secretion of IL-23 [18]. Although shikonin produces a significant therapeutic effect, its limited aqueous dissolubilty and poor bioavailability make it difficult to reach an effective therapeutic concentration through the skin. This limits its efficacy after topical administration.

Nanotechnology is used for improving the solubility and permeability of drugs, and for enhancing the affinity of the skin barrier [19–21]. Biodegradable nanoparticles have attracted much attention due to their good degradability and biocompatibility. Poly-(-lactic-co-glycolic acid) (PLGA), a biodegradable copolymer approved by FDA, is used for preparing nanoparticles [22,23]. It forms a reservoir in the skin when a drug is wrapped in it, enhances skin permeability of the drug, increases drug action time, and improves the stability of the drug [24,25].

In a study, Norfloxacin (NFX)-laden PLGA nanoparticles were formulated using a modification of the double-emulsion/solvent evaporation procedure, in order to improve the water dissolubility and pre-corneal drainage of the drug [26]. An antitumor combinatorial approach has been developed by Li et al. using piperine-loaded glycyrrhizic acid- and PLGA-based nanoparticles modified with transferrin. These approaches resulted in better solubility, enhanced delivery and improved uptake of drugs by tumor cells [27]. Curcumin has produced remarkable efficacy in the treatment of psoriasis, but its low efficiency of penetration through the stratum corneum remains a major challenge to its transdermal delivery. However, when curcumin is incorporated into PLGA nanoparticles for topical administration, the smaller particle size makes it easier for it to penetrate the skin barrier [28].

In this study, shikosin-loaded PLGA nanoparticle hydrogel was prepared and used to deliver the bioactive drug to the epidermis of psoriasis mice through local topical administration. A psoriasis mouse model was employed for determination of the therapeutic advantages of the topical administration, while the cell proliferation and specific uptake mechanisms were investigated using *in vitro* models. The aim of this study was to evolve a new technology of topical preparations with significant efficacy, minimal side effects, and better patient compliance, for use in the accurate clinical treatment of psoriasis.

2. Materials and methods

2.1. Materials

Shikonin (SH, ≥98 % pure) and Cyanine 5.5 were products of Xi'an Ruixi Co. Ltd, China. An equimolar mixture of lactic acid and glycolate (PLGA; 8 kDa) was product of Shanghai Leon Chemical Ltd., China. Polyvinyl alcohol 1788 with 88 % degree of alcoholysis and polymerization degree of 1 700, were obtained from Guidechem, Beijing, China. Sichuan Mingxin Pharm. Co. was the source of 5 % Imiquimod (IMQ) cream, while DMEM and FBS were products of Corning, USA. Cytokines for TNF-α were bought from MedChemExpress, USA. Cell counting kit (CCK)-8 was purchased from Bairuiji Co. Ltd., while MTT was obtained from Biyuntian Co. Ltd., Shanghai. Kits for RT-PCR and RNA extraction were products of Invitrogen, USA. Rabbit-derived 1^{o} immunoglobulins against p65, p-p65, and NAPDH were products of Abcam. Dexamethasone ointment (DEX) was bought from Huarun Sanjiu Co. Ltd., Shenzhen, China. All the solvents employed in this research were of analytical grade.

2.2. Animals and cells

Healthy male BALB/c mice aged 4–6 weeks and weighing 20–22 g, were purchased from Huafukang Biotechnology Co. Ltd. in Beijing, China. All laboratory procedures employed for mice received due approval from the Animal Ethical Authority of the Beijing Institute of TCM *vide* approval No. 2023-02-91. Human immortalized keratinocytes (HaCaT) were obtained from the Chinese Academy of Medical Sciences/Peking Union Medical College, Beijing. The HaCaT cells were grown at 37 °C in a high-glucose-DMEM containing 10 % (v/v) FBS in a humidified 5 % CO_2 incubator.

2.3. Preparation of shikonin PLGA NPs

Shikonin (2 mg) and 100 mg PLGA were dissolved in 3 mL dichloromethane and sonicated to obtain the organic phase. Then, 5 % PVA solution in water was prepared as the aqueous phase. The organic solution was added to the PVA solution, and the mixture was stirred on a magnetic mixer until it became transparent. Shikonin PLGA nanoparticles (SH-NPs) obtained after centrifuging at 12,000 g for 25 min, were washed thrice in deionized water. Finally, SH-NPs were freeze-dried.

2.4. Preparation of SH-gel and SH-NPs-gel

Capom 934 (2 % w: w) was added to distilled water to expand it thoroughly, followed by pH adjustment to 6.8 using 0.1 % NaOH. This was followed by addition of shikonin (20 mg) or SH-NPs (200 mg), and the mixture was magnetically stirred at the speed of 800 g until the drug was evenly distributed in the gel. The resultant SH-gel and SH-NP gel were used in subsequent studies.

2.5. Characterization of SH-NPs

2.5.1. Size and Zeta potential (ZP)

A 10:1 dilution of SH-NPs solution (1 mg) was prepared in distilled water. Then, Malvern particle size analyzer (Malvern, UK) was used for determination of the ZP and particle size of the diluted SH-NPs solution.

2.5.2. Morphological examination of SH-NPs using transmission electrom microscope (TEM)

The solution of SH-NPs was filtered through a 0.45 μm membrane and then dropped into a copper net covered with a supporting film. After natural drying, 2 % phosphotungstic acid solution was added to the solution. After staining for 2–3 min, it was examined and photographed under a TEM (JEM-2100F, Tokyo).

2.5.3. Drug-loading capacity and encapsulation efficiency

To release the drug from nanoparticles, 1 mg of SH-NPs was dissolved in dichloromethane, and the mixture was dissolved using ultrasound. Then, the dichloromethane was evaporated in a water bath, and the drug was dissolved in methanol. Then, the concentration of SH was determined in a UV–Vis spectrophotometer (Hitachi, Japan). The drug loading and encapsulation efficiency were measured and calculated using the following formula:

$$\text{Drug loading capacity } (\%) = \frac{\text{Weight of SH in NPs}}{\text{Total weight of NPs}} \times 100$$

$$\text{Encapsulation efficiency } (\%) = \frac{\text{Weight of SH in NPs}}{\text{Weight of SH fed}} \times 100$$

2.5.4. X-Ray diffraction

The sample was ground into powder in a mortar, and some of the powder was put into the sample tank. After pressing the surface of the glass plate, the sample was analyzed in the X-Ray diffractometer (Purkinje General, Beijing, China) at Cu-Kα wavelength (λ) of 1.541 nm, voltage of 40 kv, tube current of 40 mA, and scanning speed of 2° per min.

2.5.5. Fourier transform infrared spectroscopy (FTIR) analysis

The SH-NPs and spectral grade potassium bromide powder were mixed and ground at an appropriate mass ratio. After grinding evenly, the powder was pressed into a tablet and scanned in FTIR (Nicolet iS50, Waltham, MA USA) at a scanning range of 4000–400 cm^{-1}.

2.5.6. Differential scanning calorimetry (DSC)

The DSC was performed with DSC1 Stare system (MettlerToledo, Zurich CH). Appropriate amounts of SH, SH-NPs and their physical mixture were weighed. Each sample was encapsulated with a lid, placed on a flat-bottomed aluminum plate, and heated to a temperature range of 25–200 °C at a heating rate of 10 °C/min in a nitrogen atmosphere at a flow rate of 50 mL/min.

2.5.7. In vitro drug release

The dialysis bag diffusion method was used to assess the *in vitro* drug release behavior of SH-NPs [29,30]. The SH-NPs were dispersed in 2 mL of deionized water and transferred to a dialysis bag. After sealing, the mixture was put into a PBS solution of pH 7.4 containing 5 % polysorbate 80 and shaken in a 37 °C H_2O bath at 100 g. Then, 1 mL samples were taken out from the receptor compartment at 0.5, 1, 2, 4, 6, 8, 12, 48 h and added to an equal volume of fresh release medium. The absorbances of the collected samples were determined in a UV–Vis spectrophotometer at 516 nm, and the cumulative percentage release of SH from SH-NPs was calculated.

2.6. In vitro studies

2.6.1. Inductive effect of TNF-α on proliferation of HaCaT cells

The HaCaT cells (5×10^3 cells/well) were cultured in 96-well plate. Then, DMEM containing different concentrations of TNF-α (0–10 ng/ml) were added, followed by culturing for 24, 48 and 72 h. The proliferation of HaCaT cells was measured using CCK-8 assay.

2.6.2. Cell proliferation assay

The proliferation of HaCaT cells was determined using CCK-8 kit (Beyotime, Shanghai, China) in line with the instructions on the kit manual [31,32]. The effects of SH and SH-NPs (separately and combined) on cell proliferation were measured using TNF-α-treated HaCaT cells and untreated controls. The HaCaT cells (5×10^3 cells/well) were cultured in 96-well plate. Then, the cells were treated with SH and SH-NPs for 4 h. Subsequently, TNF-α (10 ng/mL) was added, followed by culturing for 24 h, after which 10 μl CCK-8 assay reagent was put into every well. The absorbance of solution in each well was measured at 450 nm in a microplate instrument (Thermo Scientific Multiskan GO, USA), after a 2-h incubation.

2.6.3. Cellular uptake of NPs

The HaCaT cells were inoculated into 24-well plate at a density of 1×10^6 cells/well and cultured overnight. Thereafter, the cells were treated with Cy5.5 PLGA NPs and cultured for 4 h. Then, TNF-α (10 ng/ml) was added, followed by incubation for 24 h. Thereafter, PBS was used to rinse the cells, followed by a 10 min fixation with 4 % paraformaldehyde. Following cell rinsing in PBS (twice), cells were subjected to 5-min staining with DAPI, rinsed three times with PBS, and examined under a fluorescence microscope (Olympus, Japan).

2.6.4. Apoptosis of HaCaT cells

The HaCaT cells (1×10^5 cells/well) were seeded into 6-well plate. Then, fresh medium samples containing SH and SH-NPs (1 μM and 2 μM, respectively) were added into separate wells, followed by incubation for 4 h. Subsequently, TNF-α (10 ng/ml) was put into every well, followed by culturing for 24 h. Thereafter, the cells were trypsinized, washed twice with PBS and centrifuged (3000 g) for 10 min. The cell pellet was taken up in 295 μL of binding buffer, and counterstained in a dark chamber for 20 min with Annexin V-FITC and propidium iodide. Then, the stained cells were analyzed using a flow cytometer (Becton Dickinson, USA).

2.6.5. Western blot assay

Western blotting was used to determine the effect of SH on the expressions of apoptotic proteins in HaCaT cells [33,34]. The HaCaT cells were treated with SH and SH-NPs (1 μM and 2 μM) for 4 h. Subsequently, the cells were exposed to TNF-α (10 ng/ml) for 24 h. Then, total protein extraction was done by lysing the HaCaT cells with RIPA buffer at 4 °C for 25 min. The lysate was rinsed once using PBS, and with RIPA buffer for 30 min. The concentrations of total protein samples obtained after centrifugation of the lysate were measured using BCA kit. Then, equal amounts of protein samples were subjected to 10 % SDS-PAGE, followed by transfer onto PVDF membranes (Millipore, USA) which were thereafter blocked in 5 % defatted milk. The PVDF membranes were subjected to overnight incubation with primary antibodies for anti-p65 (1:1000) and anti-p-p65 (1:1000) at 4 °C (Abcam, USA), and subsequently probed using horse radish peroxidase-labeled 2^o immunoglobulins (diluted 1:8000) for 2 h at 25 °C. Blot detection was done using enhanced chemiluminescence (Thermo Fisher Scientific, USA). The internal reference was GAPDH. All experiments were independently repeated three times.

2.7. In vivo studies

2.7.1. Psoriasis mouse model and grouping

The BALB/C mice were randomly divided into seven groups: control group, model group, dexamethasone group, high-dose SH group (0.2 mg/g), low-dose SH group (0.1 mg/g), high-dose SH-NPs group (0.2 mg/g), and low-dose SH-NPs (0.1 mg/g), with 6 mice in each group. A psoriasis mouse model was established using imiquimod treatment [35]. The mice were anesthetized *via* intraperitoneal injection of 1 % pentobarbital sodium (80 mg/kg), and the hair was removed from an area of 2 cm × 3 cm on the back of each mouse. Thereafter, the mice were housed individually. All mice other than blank control mice, were treated with 5 % imiquimod which was topically applied once daily on the shaved skin area on the back. The skin of the treated mice showed erythema, scales, and infiltrative psoriasis-like lesions, all of which gradually worsened daily, indicating successful establishment of the psoriasis model. Six hours after administration, the formulations were applied on the back skin of each mouse. Mice in control and the model cohorts were treated with carbomer blank matrix gel.

2.7.2. Evaluation of area of psoriasis (PASI)

An objective of scoring for PASI was employed for determination of extent of skin inflammation. This comprised assesement of erythema, thickness and scaling. All the parameters were separately rated on a 0–4 scale, with scores of 1, 2, 3 and 4 for none, slight, moderate, and significant, respectively, with total score indicating degree of inflammatory lesions. The total score was obtained by summing up scores in respect of the 3 parameters, with a maximum score of 12 points. A PASI score line chart was plotted and used to determine dynamic changes in mouse skin lesions over time.

2.7.3. Histopathology in the skin samples

After 6 days, the mice were euthanized, and skin samples were taken and subjected to formalin fixation. Then, the samples were parrafinized and microtomed, followed by routine staining with H & E. Then, the tissue sections were examined under an inverted microscope (Leeds Precision Instruments, USA) for histopathological changes in each experimental group.

2.7.4. Quantitative real-time PCR analysis

The mRNA levels of proinflammatory cytokines in the skin of psoriasis mice were determined using qRT-PCR [36,37]. On the 7th day after establishment of the psoriasis model, mouse dorsal skin samples were collected, rapidly frozen in liquid nitrogen, and kept frozen at −80 °C. The skin samples were ground to powder in pre-cooled mortar and pestle. Total RNA extraction from each of the specimens was done using TRIzol. Subsequently, the RNA samples were reverse-transcribed into cDNA using the Fastking One-Step qRT-PCR Kit. The reaction system was prepared by incubating the mixture at 37 °C for 15 min, followed by a denaturation step at 85 °C for 5 s, and then cooling to 4 °C. Finally, CFX Duet Real-Time PCR equipment was used for qRT-PCR. The relative mRNA expression levels were calculated using the $2^{-\Delta\Delta CT}$ method.

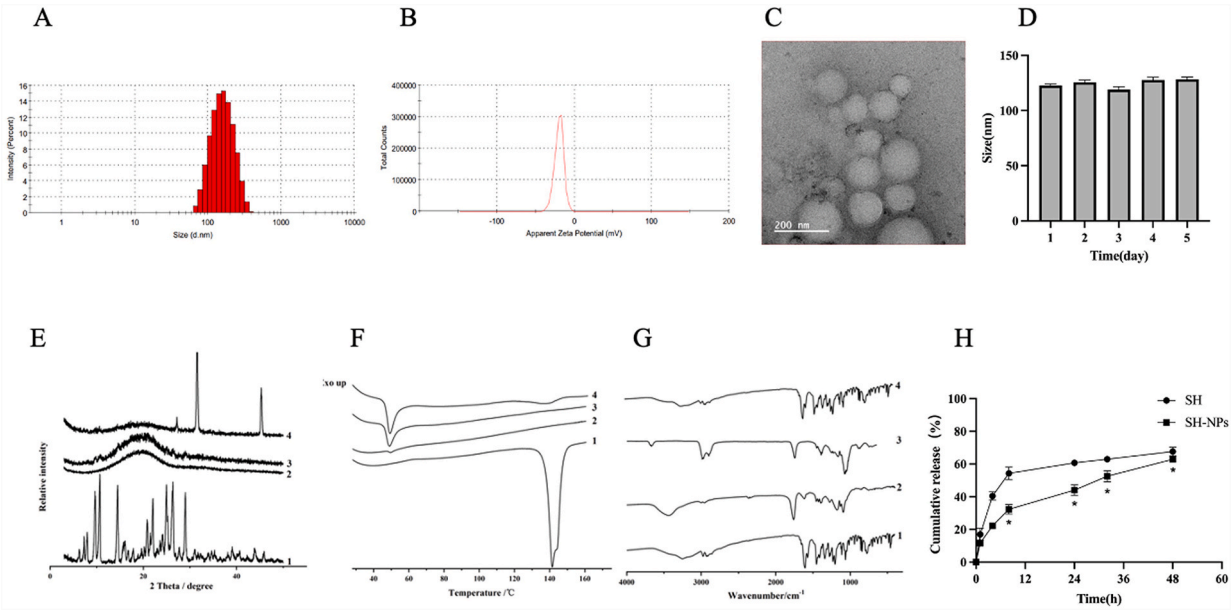

Fig. 1. Characterization of shikonin loaded nanoparticles. (A) Particle size, and (B) ZP of SH-NPs. (C) TEM diagram of SH-NPs. (D) The stability of SH-NPs. (C) The XRPD patterns (E), DSC curves (F) and FT-IR spectra (G) of different samples (1: SH, 2: SH-NPs, 3: PLGA, and 4: physical mixture). (H) Cumulative release behaviors of SH and SH-NPs.

Table 1
SH-NPs fitting release model and coefficient.

Model	Fitting equation	R^2
Zero-order equation	$M_t/M_\infty = 1.15422t + 12.941$	0.86368
First-order equation	$M_t/M_\infty = 56.27374\ (\ 1\text{-}e^{-0.10463t}\ )$	0.93837
Higuchi equation	$M_t/M_\infty = 8.74945t^{1/2} + 3.09324$	0.9855
Ritger-Peppas equation	$M_t/M_\infty = 12.66609\ (\ t^{0.41,006}\ )$	0.99393

M_∞ is accumulative drug-release at time, M_t is accumulative drug-release at time t, M_t/M_∞ is accumulative release rate at time t, t is time.

2.8. Statistical analysis

All experiments were performed in at least three independent replications, and data are expressed as mean ± SD. Statistical analysis were done using one-way ANOVA. Values of $p < 0.05$ were assumed as indicative of significant differences.

3. Results and discussion

3.1. Properties of SH-NPs

As shown in Fig. 1A & B, the poly-dispersion index and particle size of SH-NPs were measured with Malvern analyzer. The results showed that the particle size of SH-NPs was 123 ± 10.69 nm, and the PDI was 0.18 ± 0.006, while the Zeta potential was −17.63 ± 1.62 mV. The drug loading of shikonin was 7.4 %, and the entrapment efficiency was 80 %. Scanning electron microscopy was used to determine the morphology of the nanoparticles. Uniform spherical particles were observed, and the dispersion was good (Fig. 1C). This was consistent with the data of particle size analysis. The particle size of SH-NPs did not change obviously within 5 days, indicating that the SH-NPs were stable (Fig. 1D). The XRD spectrum showed that the strong absorption peak of shikonin in the nanoparticles disappeared completely, while the diffuse diffraction peak appeared (Fig. 1E), indicating that the drug was distributed in an amorphous state. The DSC results demonstrated that the melting peak of the drug disappeared (Fig. 1F). This indicates that the crystallinity of shikonin in the nanoparticles was decreased due to the coating of the PLGA carrier. The FTIR spectra of SH-NPs was basically consistent with the black nanoparticles, while the characteristic peaks of SH were not shown in SH-NPs, indicating that SH was successfully encapsulated into PLGA nanoparticles (Fig. 1G). These results indicate that the main functional groups in the drug were not modified after the preparation of the nanoparticles. Fig. 1H shows the *in vitro* release patterns of SH and SH-NPs. Shikonin exhibited the fastest release profiles, with 67.62 ± 2.57 % release at 48 h. The release curve of SH-NPs showed good slow-release profile. The cumulative release of SH-NPs within 48 h was 62.86 ± 1.66 %, indicating that PLGA coating reduced the burst release

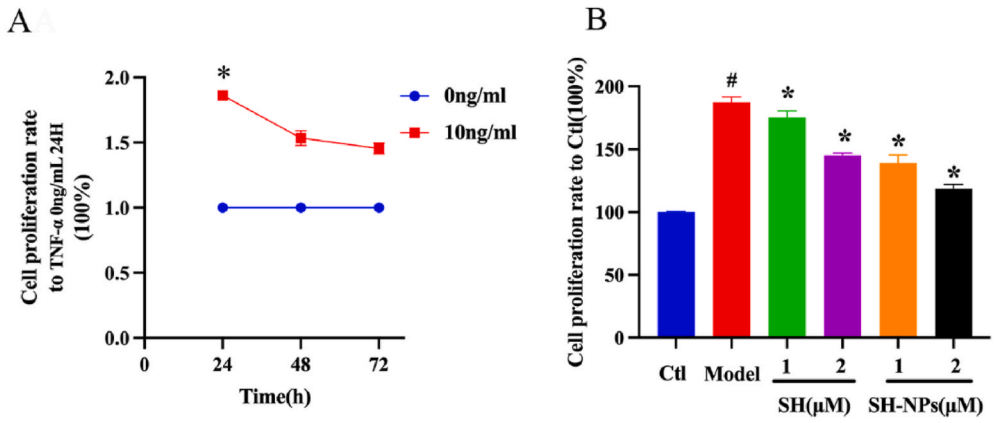

Fig. 2. Effect of SH-NPs on proliferation of HaCaT cells. (A) Effect of 24–72 h treatment on HaCaT cell viability. (B) Viability of HaCaT cells. $\#P < 0.05$, vs. control; $*p < 0.05$, vs. model.

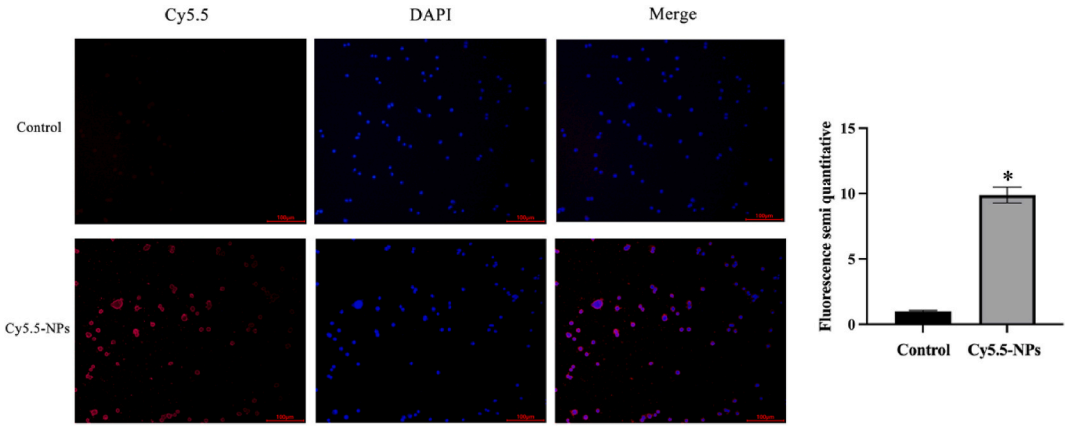

Fig. 3. Uptake of CY5.5-NPs by HaCaT cells. $*P < 0.05$, compared with control group.

effect of the drug. Mathematical models were used to study mechanism underlying the release of SH from SH-NPs. The data suggest that the drug release regularity of SH-NPs was consistent with the Ritger-Peppas model (Table 1).

3.2. *Viability of HaCaT cells*

Treatment with TNF-α induces high rate of proliferation in HaCaT cells. Therefore, the cells were exposed to TNF-α in order to establish an *in vitro* high-proliferation cell model. Compared with the untreated cells, TNF-α (10 ng/mL) effectively raised the relative population of healthy HaCaT cells to 186.1 ± 1.9 % at 24 h, indicating successful establishment of the high-proliferation cell model (Fig. 2A). The results from CCK-8 measurement showed that upon SH exposure at doses of 1 μM and 2 μM, the populations of healthy TNF-α-exposed cells were reduced to 175.3 ± 5.2 % and 145.2 ± 1.9 %, respectively. In contrast, SH-NPs reduced population of healthy TNF-α-exposed cells by approximately 139.1 ± 6.6 % and 118.6 ± 3.4 % at equivalent shikosin concentrations of 1 μM and 2 μM, respectively (Fig. 2B). These data demonstrate that high dose of SH-NPs exerted more significant inhibitory effect on TNF-α-induced cell proliferation than SH, most likely due to facilitated intake of SH-NPs by cells.

3.3. *Uptake of NPs in vitro*

The time-dependent uptake of nanoparticles and distribution and location of nanoparticles in HaCaT cells were determined using CY5.5 fluorescence probe [38,39]. The results in Fig. 3 show that the red fluorescence of nanoparticles was almost entirely located in the cytoplasm. The red fluorescence of CY5.5-NPs group in HaCaT cells was significantly stronger than that of CY5.5 group at comparable levels of CY5.5. The data suggest that the nanoparticles improved the entry of the drug into HaCaT cells.

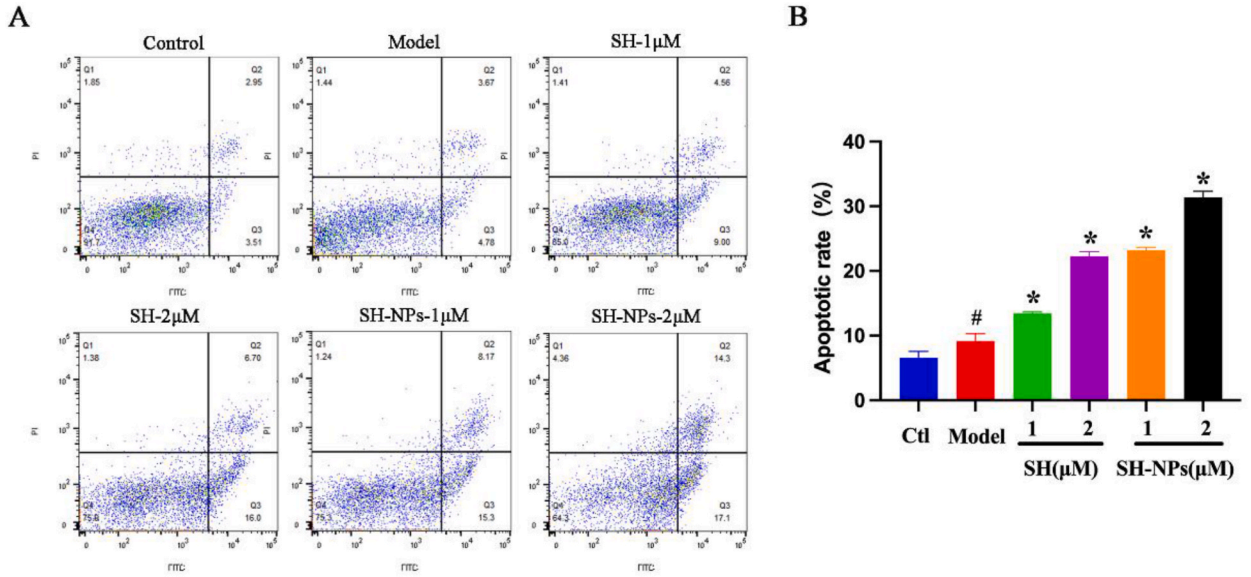

Fig. 4. Effects of SH and SH-NPs on HaCaT cellular apoptosis. (A) Scatter diagram using data from flow cytometry. (B) Initial and later apoptotic rates. Values are mean ± SD. $\#P < 0.05$, vs. control; $*p < 0.05$, vs. model.

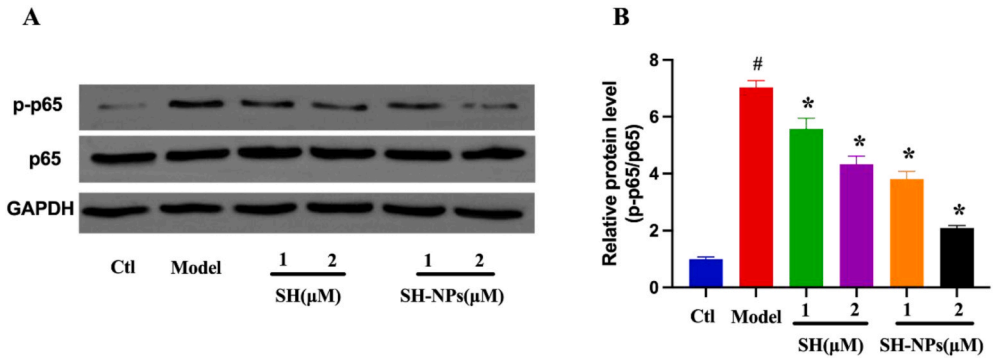

Fig. 5. The effects of SH and SH-NPs on p65 phosphorylation in HaCaT keratinocytes after stimulation with TNF-α. (A) Protein levels of p65 and p-p65. (B) Quantified protein levels based on band intensity. Results are expressed as mean ± SD (n = 3). $^{\#}P < 0.05$, compared with control group, $*P < 0.05$, compared with model group.

3.4. Apoptosis of HaCaT cells

The roles of keratinocyte apoptosis in development of the epidermis, as well as in apoptosis suppression, are major factors in psoriasis-induced epidermal thickening. When keratinocyte growth and apoptosis are not balanced, psoriasis results [40]. In this study, the apoptosis rate of HaCaT cells was quantified with Annexin V-FITC and PI dyes. The apoptosis rates of groups given shikonin at doses of 1 μM and 2 μM were 13.56 % and 22.70 %, respectively, while the apoptosis rates for SH-NPs were 23.47 % and 31.4 %, respectively (Fig. 4A). The number of living cells decreased significantly with increase in drug concentration, while the number of apoptotic cells and necrotic cells increased (Fig. 4B). In addition, compared with the free drug group, SH-NPs treatment led to increased rate of apoptosis of tumor cells and a reduction in the apoptosis rate of normal cells. These data were consistent with the results from cell viability assays using CCK-8.

3.5. Western blot results

The expression of p65 protein was determined with Western blot, in order to study the process involved in the effect of SH in HaCaT cells. The HaCaT cells were pretreated with SH and SH-NPs at the same concentration for 6 h, after which they were stimulated with TNF-α (10 ng/mL) for 24 h. The protein levels of p65 and p-p65 were determined using Western blot assay. Compared with the control group, the TNF-α treatment significantly induced the phosphorylation of p-65, which indicates that the NF-κB signal route was activated (Fig. 5A). In contrast, the protein levels of p65 and p-p65 were downregulated in a dose-dependent manner after 24 h of

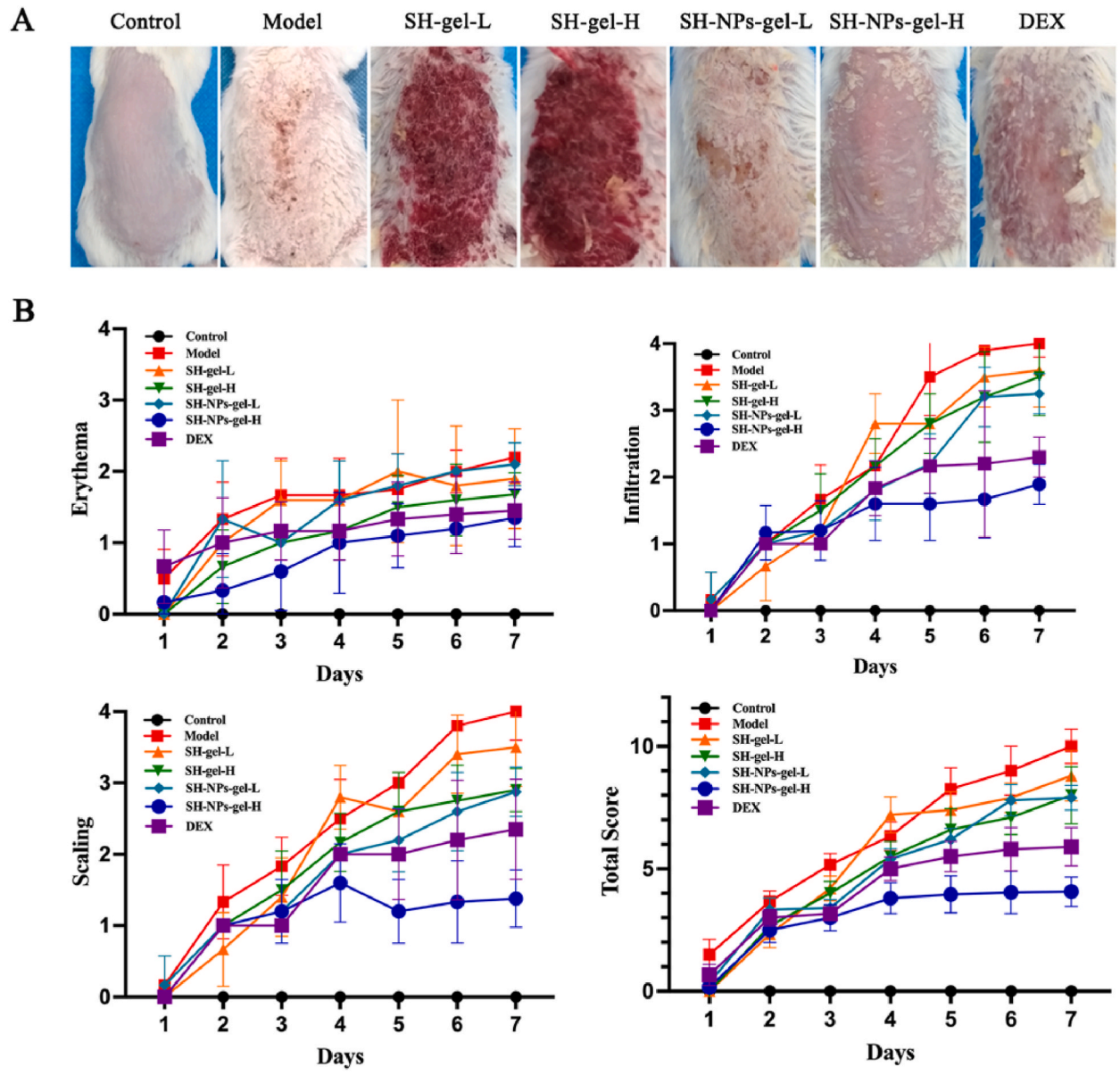

Fig. 6. The effects of SH-gel and SH-NPs-gel on IMQ-induced psoriasis mice. (A) Macroscopic image of mouse skin after 7 days. (B) Scores on erythema, scaling, and infiltration of the back skin, as well as cumulative PASI scores. For each cohort, values are mean ± SD of results for six mice.

administration of SH and SH-NPs, relative to model group (Fig. 5B). These results indicate that the nanoparticles significantly enhanced the inhibitory effect of SH on viability of HaCaT cells, when compared with the free drug.

3.6. Macroscopic examination of dorsal tissue

In the control group, the dorsal skin of mice appeared smooth and pale-pink. In the model group, the mice exhibited psoriasis-like skin lesions characterized by gradual accumulation of scales, thickening, and infiltration, after 2 days of establishment of the psoriasis model. However, relative to the model group, mice in treated cohorts showed reductions in skin erythema, scaling, and infiltration, during the same period (Fig. 6A). The dynamic changes in mouse skin lesions over time were measured using PASI scores (Fig. 6B). Mice in control cohort showed no changes in PASI values, while mice treated with IMQ had evidence of scaling and erythema. Compared with other treatments, SH-NPs-gel-H produced excellent suppression of psoriasis, with comparable scores in high-dose SH-NP-gel and DEX groups.

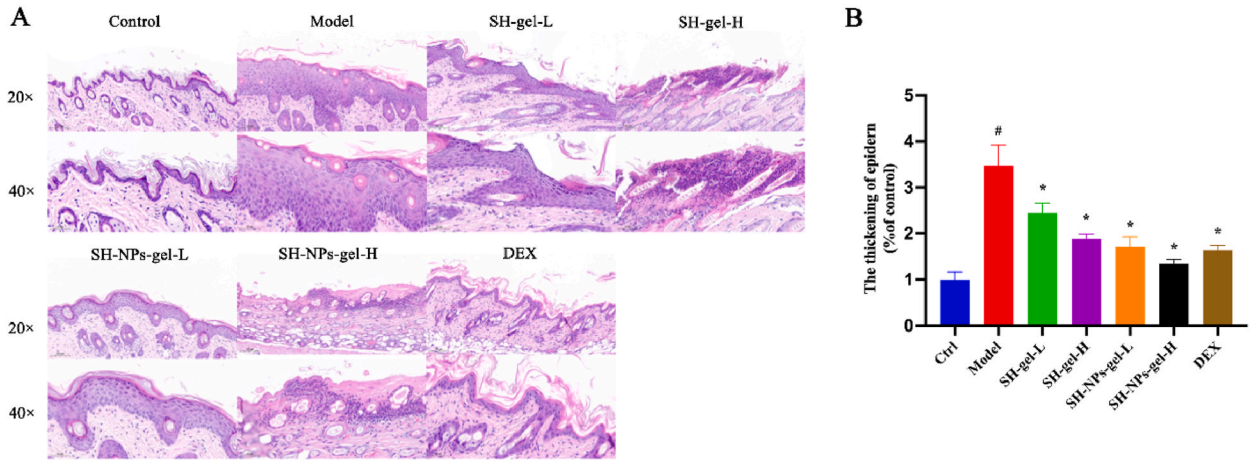

Fig. 7. (A) Photomicrographs of mouse skin sections (H & E; × 200 or × 400); and related skin thicknesses (B). $^{\#}P < 0.05$, compared with control group, $^{*}p < 0.05$, compared with model group.

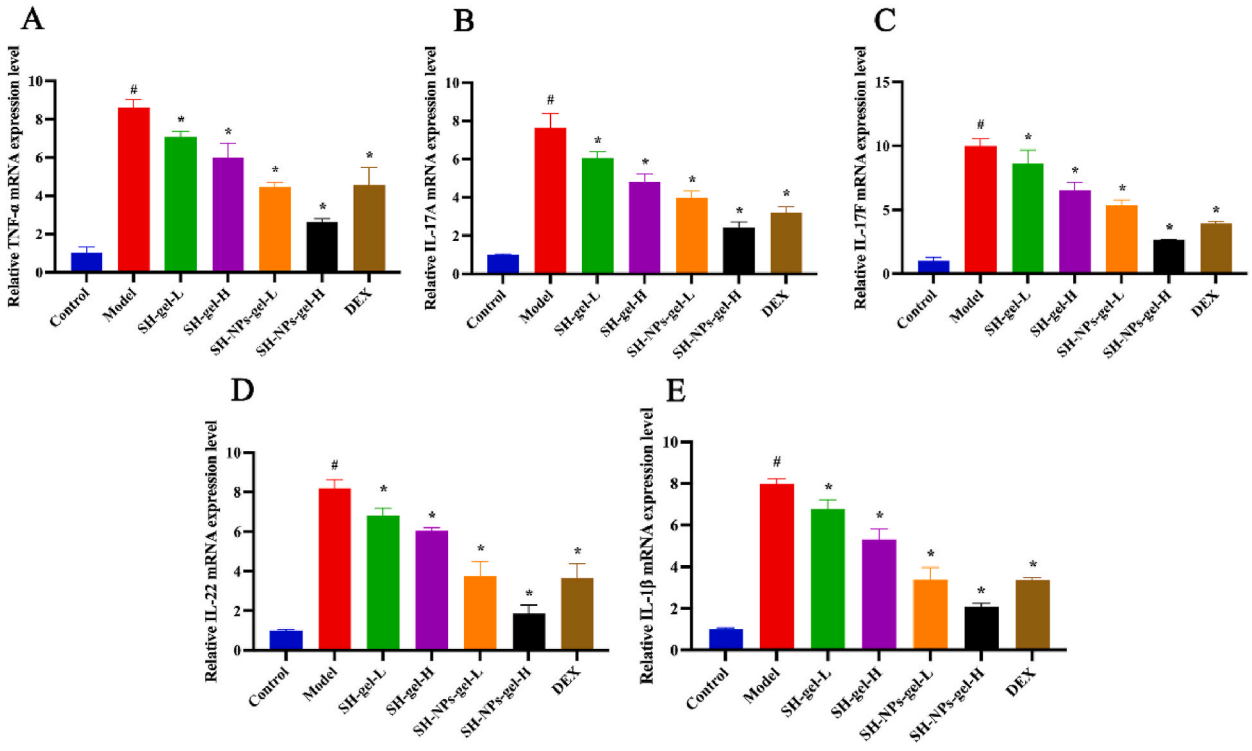

Fig. 8. Effects of SH-gel and SH-NPs-gel on mRNA levels of pro-inflammatory factors in IMQ-mediated mouse model of psoriasis. mRNA values of TNF-α (A), IL-17A (B), IL-17F (C), IL-22 (D) and IL-1β (F) in skin lesion. $^{\#}P < 0.05$, vs. control; $^{*}p < 0.05$, vs. model mice.

3.7. Skin histopathology

Further confirmation of the therapeutic effect of SH-NP formulations on psoriasis was obtained through H & E staining [41,42]. Histological changes in skin samples from different groups are shown in Fig. 7A. Mice in the model group exhibited significant epidermal thickening, excessive keratinization, and incomplete keratinization, along with increased infiltration of inflammatory cells in the dermis, relative to control mice. Mice in the treatment groups had noticeable reductions in epidermal thickness and decreased infiltration of inflammatory cells, with the SH-NP-gel-H group having the most significant therapeutic effect (Fig. 7B).

3.8. Relative expression levels of the inflammation cytokine mRNA in mouse skin lesions

Psoriasis, a skin condition due to chronic inflammation, is marked by excessive activation of inflammation [43]. The inflammatory mediators (IL-17A, IL-17F, IL-22, IL-1β, and TNF-α) play crucial roles in the occurrence and development of psoriasis-associated inflammation and excessive proliferation of keratinocytes [44,45]. Results from qRT-PCR showed significant up-regulation of mRNA concentrations of pro-inflammatory cytokines in psoriasis mice (Fig. 8A–E). However, all the SH treatment groups exhibited downregulation of these cytokines, with the most potent inhibitory effect observed in the SH-NPs-gel-H group.

4. Conclusion

Poor solubility and poor bioavailability limit the clinical application of shikonin. In this study, shikonin PLGA nanoparticles were synthesized for the first time using emulsion solvent evaporation method. Under optimal formulation, the drug loading of SH-NPs reached 7.4 %, and the encapsulation efficiency was 80 %. The nanoparticles were sphere-shaped, with a narrow-size distribution. The cumulative liberation of SH-NPs within 8 h was 32.33 ± 2.91 %, indicating that SH-NPs reduced the sudden release of the free drug. Compared with model group, the two different doses of SH-NPs decreased TNF-α-induced the proliferation of HaCaT cells by approximately 139.1 ± 6.6 % and 118.6 ± 3.4 %, respectively. Moreover, SH-NPs enhanced *in vitro* permeation rate of the drug in the cells. The impacts of shikonin were linked to reductions in protein expressions of p65 and p-p65. Moreover, shikonin ameliorated the severity of skin lesion and decreased the levels of associated cytokines in the psoriatic mice. These data indicate that shikonin has a promising potential for use in the design of drugs against psoriasis. The SH-NPs gel may be used in the form of topical administration in the treatment of psoriasis.

Funding

This work was supported by the National Natural Science Foundation of China (Grant No. 82305244).

Ethical statement

All animal experiments in this study were approved by the Animal Ethics Committee of the Beijing Institute of Traditional Chinese Medicine (approval no.: 2023-02-91).

Data availability statement

Data will be made available on reasonable request.

Institutional review board statement

Not applicable.

CRediT authorship contribution statement

Jing Fu: Validation, Investigation, Conceptualization. **Longtai You:** Formal analysis, Data curation. **Daohan Sun:** Validation. **Lu Zhang:** Writing – original draft, Data curation. **Jingxia Zhao:** Writing – original draft, Supervision. **Ping Li:** Supervision.

Declaration of competing interest

The authors declare that they have no known competing financial interests or personal relationships that could have appeared to influence the work reported in this paper.

Appendix A. Supplementary data

Supplementary data to this article can be found online at https://doi.org/10.1016/j.heliyon.2024.e31909.

References

[1] R.S. Gangwar, J.E. Gudjonsson, N.L. Ward, Mouse models of psoriasis: a comprehensive review, J. Invest. Dermatol. 142 (3 Pt B) (2022) 884–897.
[2] A.M. Man, M.S. Orăsan, O.A. Hoteiuc, M.C. Olănescu-Vaida-Voevod, T. Mocan, Inflammation and psoriasis: a comprehensive review, Int. J. Mol. Sci. 24 (22) (2023) 16095.
[3] A. Chiricozzi, P. Romanelli, E. Volpe, G. Borsellino, M. Romanelli, Scanning the immunopathogenesis of psoriasis, Int. J. Mol. Sci. 19 (1) (2018) 179.
[4] J. Fuentes-Duculan, K.M. Bonifacio, J.E. Hawkes, N. Kunjravia, I. Cueto, X. Li, J. Gonzalez, S. Garcet, J.G. Krueger, Autoantigens ADAMTSL5 and LL37 are significantly upregulated in active Psoriasis and localized with keratinocytes, dendritic cells and other leukocytes, Exp. Dermatol. 26 (11) (2017) 1075–1082.

[5] A.W. Armstrong, C. Read, Pathophysiology, clinical presentation, and treatment of psoriasis: a review, JAMA 323 (19) (2020) 1945–1960.
[6] O.Y. Elkhawaga, M.M. Ellety, S.O. Mofty, M.S. Ghanem, A.O. Mohamed, Review of natural compounds for potential psoriasis treatment, Inflammopharmacology 31 (3) (2023) 1183–1198.
[7] X. Zhou, Y. Chen, L. Cui, Y. Shi, C. Guo, Advances in the pathogenesis of psoriasis: from keratinocyte perspective, Cell Death. Dis. 13 (1) (2022) 81.
[8] C. Albanesi, S. Madonna, P. Gisondi, G. Girolomoni, The interplay between keratinocytes and immune cells in the pathogenesis of psoriasis, Front. Immunol. 9 (2018) 1549.
[9] E.A. Madawi, A.R. Al Jayoush, M. Rawas-Qalaji, H.E. Thu, S. Khan, M. Sohail, A. Mahmood, Z. Hussain, Polymeric nanoparticles as tunable nanocarriers for targeted delivery of drugs to skin tissues for treatment of topical skin diseases, Pharmaceutics 15 (2) (2023) 657.
[10] M. Ferreira, L. Barreiros, M.A. Segundo, T. Torres, M. Selores, S.A. Costa Lima, S. Reis, Topical co-delivery of methotrexate and etanercept using lipid nanoparticles: a targeted approach for psoriasis management, Colloids Surf. B Biointerfaces 159 (2017) 23–29.
[11] Q. Zhou, B. Chen, X. Chen, Y. Wang, J. Ji, M. Kizaibek, X. Wang, L. Wu, Z. Hu, X. Gao, N. Wu, D. Huang, X. Xu, W. Lu, X. Cai, Y. Yang, J. Ye, Q. Wei, J. Shen, P. Cao, Arnebiae Radix prevents atrial fibrillation in rats by ameliorating atrial remodeling and cardiac function, J. Ethnopharmacol. 248 (2020) 112317.
[12] J. Sun, S. Wang, Y. Wang, R. Wang, K. Liu, E. Li, P. Qiao, L. Shi, W. Dong, L. Huang, L. Guo, Phylogenomics and genetic diversity of Arnebiae radix and its allies (arnebia, boraginaceae) in China, Front. Plant Sci. 13 (2022) 920826.
[13] L. Zhu, K. Li, M. Liu, K. Liu, S. Ma, W. Cai, Anti-cancer research on Arnebiae radix-derived naphthoquinone in recent five years, recent pat, Anticancer Drug Discov 17 (3) (2022) 218–230.
[14] L. Zhu, S. Ma, K. Li, P. Xiong, S. Qin, W. Cai, Systematic screening of chemical constituents in the traditional Chinese medicine Arnebiae radix by UHPLC-Q-exactive orbitrap mass spectrometry, Molecules 27 (9) (2022) 2631.
[15] J. Wang, L. Liu, X.Y. Sun, S. Zhang, Y.Q. Zhou, K. Ze, S.T. Chen, Y. Lu, X.C. Cai, J.L. Chen, Y. Luo, Y. Ru, B. Li, X. Li, Evidence and potential mechanism of action of lithospermum erythrorhizon and its active components for psoriasis, Front. Pharmacol. 13 (2022) 781850.
[16] Y.J. Yu, Y.Y. Xu, X.O. Lan, X.Y. Liu, X.L. Zhang, X.H. Gao, L. Geng, Shikonin induces apoptosis and suppresses growth in keratinocytes via CEBP-δ upregulation, Int. Immunopharm. 72 (2019) 511–521.
[17] C. Guo, J. He, X. Song, L. Tan, M. Wang, P. Jiang, Y. Li, Z. Cao, C. Peng, Pharmacological properties and derivatives of shikonin-A review in recent years, Pharmacol. Res. 149 (2019) 104463.
[18] X. Zhang, J. Li, Y. Yu, P. Lian, X. Gao, Y. Xu, L. Geng, Shikonin controls the differentiation of CD4+CD25+ regulatory T cells by inhibiting AKT/mTOR pathway, Inflammation 42 (4) (2019) 1215–1227.
[19] M. Rahman, S. Beg, S. Akhter, Conventional formulations, challenges, and nanomedicines in infective and non-infective skin diseases therapy, Recent Pat. Anti-Infect. Drug Discov. 14 (1) (2019) 5–6.
[20] S. Parveen, M. Ahmed, S. Baboota, J. Ali, An innovative approach in nanotechnology-based delivery system for the effective management of psoriasis, Curr. Pharmaceut. Des. 28 (13) (2022) 1082–1102.
[21] G.S. Gomes, L.A. Frank, R.V. Contri, M.S. Longhi, A.R. Pohlmann, S.S. Guterres, Nanotechnology-based alternatives for the topical delivery of immunosuppressive agents in psoriasis, Int. J. Pharm. 631 (2023) 122535.
[22] A.K. Shakya, M. Al-Sulaibi, R.R. Naik, H. Nsairat, S. Suboh, A. Abulaila, Review on PLGA polymer based nanoparticles with antimicrobial properties and their application in various medical conditions or infections, Polymers 15 (17) (2023) 3597.
[23] J.C. Ma, T. Luo, B. Feng, Z. Huang, Y. Zhang, H. Huang, X. Yang, J. Wen, X. Bai, Z.K. Cui, Exploring the translational potential of PLGA nanoparticles for intra-articular rapamycin delivery in osteoarthritis therapy, J. Nanobiotechnol. 21 (1) (2023) 361.
[24] P. Carter, B. Narasimhan, Q. Wang, Biocompatible nanoparticles and vesicular systems in transdermal drug delivery for various skin diseases, Int. J. Pharm. 555 (2019) 49–62.
[25] M.F. Aldawsari, F.K. Alkholifi, A.I. Foudah, M.H. Alqarni, A. Alam, M.A. Salkini, S.H. Sweilam, Gallic-acid-loaded PLGA nanoparticles: a promising transdermal drug delivery system with antioxidant and antimicrobial agents, Pharmaceuticals 16 (8) (2023) 1090.
[26] R.M. Gebreel, N.A. Edris, H.M. Elmofty, M.I. Tadros, M.A. El-Nabarawi, D.H. Hassan, Development and characterization of PLGA nanoparticle-laden hydrogels for sustained ocular delivery of Norfloxacin in the treatment of Pseudomonas keratitis: an experimental study, Drug Des. Dev. Ther. 15 (2021) 399–418.
[27] S. Li, J. Guo, Z. Tian, J. Chen, G. Gou, Y. Niu, L. Li, J. Yang, Piperine-loaded glycyrrhizic acid- and PLGA-based nanoparticles modified with transferrin for antitumor : piperine-loaded glycyrrhizic acid- and PLGA-based nanoparticles, AAPS PharmSciTech 22 (7) (2021) 239.
[28] L. Sun, Z. Liu, L. Wang, D. Cun, H.H.Y. Tong, R. Yan, X. Chen, R. Wang, Y. Zheng, Enhanced topical penetration, system exposure and anti-psoriasis activity of two particle-sized, curcumin-loaded PLGA nanoparticles in hydrogel, J. Contr. Release 254 (2017) 44–54.
[29] M. Yu, W. Yuan, D. Li, A. Schwendeman, S.P. Schwendeman, Predicting drug release kinetics from nanocarriers inside dialysis bags, J. Contr. Release 315 (2019) 23–30.
[30] B. Balzus, M. Colombo, F.F. Sahle, G. Zoubari, S. Staufenbiel, R. Bodmeier, Comparison of different in vitro release methods used to investigate nanocarriers intended for dermal application, Int. J. Pharm. 513 (1–2) (2016) 247–254.
[31] L. Li, C. Liu, J. Fu, Y. Wang, D. Yang, B. Peng, X. Liu, X. Han, Y. Meng, F. Feng, X. Hu, C. Qi, Y. Wang, Y. Zheng, P. Li, CD44 targeted indirubin nanocrystal-loaded hyaluronic acid hydrogel for the treatment of psoriasis, Int. J. Biol. Macromol. 243 (2023) 125239.
[32] P. Liu, B. Fan, B. Othmane, J. Hu, H. Li, Y. Cui, Z. Ou, J. Chen, X. Zu, m6A-induced lncDBET promotes the malignant progression of bladder cancer through FABP5-mediated lipid metabolism, Theranostics 12 (14) (2022) 6291–6307.
[33] H. Peng, L. You, C. Yang, K. Wang, M. Liu, D. Yin, Y. Xu, X. Dong, X. Yin, J. Ni, Ginsenoside Rb1 attenuates triptolide-induced cytotoxicity in HL-7702 cells via the activation of Keap1/Nrf2/ARE pathway, Front. Pharmacol. 12 (2022) 723784.
[34] M. Gao, Y. Li, W. Ho, C. Chen, Q. Chen, F. Li, M. Tang, Q. Fan, J. Wan, W. Yu, X. Xu, P. Li, X.Q. Zhang, Targeted mRNA nanoparticles ameliorate blood-brain barrier disruption postischemic stroke by modulating microglia polarization, ACS Nano 18 (4) (2024) 3260–3275.
[35] L. Van der Fits, S. Mourits, J.S. Voerman, M. Kant, L. Boon, J.D. Laman, F. Cornelissen, A.M. Mus, E. Florencia, E.P. Prens, E. Lubberts, Imiquimod-induced psoriasis-like skin inflammation in mice is mediated via the IL-23/IL-17 axis, J. Immunol. 182 (9) (2009) 5836–5845.
[36] F. Zhou, J. Mei, X. Han, H. Li, S. Yang, M. Wang, L. Chu, H. Qiao, T. Tang, Kinsenoside attenuates osteoarthritis by repolarizing macrophages through inactivating NF-κB/MAPK signaling and protecting chondrocytes, Acta Pharm. Sin. B 9 (5) (2019) 973–985.
[37] M. Ni, J. Zhou, Z. Zhu, Q. Xu, Z. Yin, Y. Wang, Z. Zheng, H. Zhao, Shikonin and cisplatin synergistically overcome cisplatin resistance of ovarian cancer by inducing ferroptosis via upregulation of HMOX1 to promote Fe2+ accumulation, Phytomedicine 112 (2023) 154701.
[38] H.S. Lee, N.W. Kang, H. Kim, D.H. Kim, J.W. Chae, W. Lee, G.Y. Song, C.W. Cho, D.D. Kim, J.Y. Lee, Chondroitin sulfate-hybridized zein nanoparticles for tumor-targeted delivery of docetaxel, Carbohydr. Polym. 253 (2021) 117187.
[39] H.J. Cho, S.J. Park, Y.S. Lee, S. Kim, Theranostic iRGD peptide containing cisplatin prodrug: dual-cargo tumor penetration for improved imaging and therapy, J. Contr. Release 300 (2019) 73–80.
[40] R. Zhang, Y.H. Wang, X. Shi, J. Ji, F.Q. Zhan, H. Leng, Sortilin regulates keratinocyte proliferation and apoptosis through the PI3K-AKT signaling pathway, Life Sci. 278 (2021) 119630.
[41] M.H. Zulfakar, A. Alex, B. Povazay, W. Drexler, C.P. Thomas, R.M. Porter, C.M. Heard, In vivo response of GsdmA3Dfl/+ mice to topically applied anti-psoriatic agents: effects on epidermal thickness, as determined by optical coherence tomography and H&E staining, Exp. Dermatol. 3 (3) (2011) 269–272.
[42] B. Chen, R. Huang, W. Zeng, W. Wang, Y. Min, Nanocodelivery of an NIR photothermal agent and an acid-responsive TLR7 agonist prodrug to enhance cancer photothermal immunotherapy and the abscopal effect, Biomaterials 305 (2023) 122434.
[43] T. Tashiro, Y. Sawada, Psoriasis and systemic inflammatory disorders, Int. J. Mol. Sci. 23 (8) (2022) 4457.
[44] R.K. Gupta, D.T. Gracias, D.S. Figueroa, H. Miki, J. Miller, K. Fung, F. Ay, L. Burkly, M. Croft, TWEAK functions with TNF and IL-17 on keratinocytes and is a potential target for psoriasis therapy, Sci. Immunol. 6 (65) (2021) eabi8823.
[45] L. Zhang, X. Ma, R. Shi, L. Zhang, R. Zhao, R. Duan, Y. Qin, S. Gao, X. Li, J. Duan, J. Li, Allicin ameliorates imiquimod-induced psoriasis-like skin inflammation via disturbing the interaction of keratinocytes with IL-17A, Br. J. Pharmacol. 180 (5) (2023) 628–646.